Earth Surf. Dynam. Discuss., 1, 711–743, 2013
www.earth-surf-dynam-discuss.net/1/711/2013/
doi:10.5194/esurfd-1-711-2013

Earth Surface Dynamics Discussions
Open Access

Morphodynamic regime change induced by riparian vegetation in a restored lowland stream

J. P. C. Eekhout and A. J. F. Hoitink

Hydrology and Quantitative Water Management Group, Wageningen University, Wageningen, the Netherlands

Received: 15 October 2013 – Accepted: 31 October 2013 – Published: 15 November 2013

Correspondence to: J. P. C. Eekhout (joris.eekhout@wur.nl) and
A. J. F. Hoitink (ton.hoitink@wur.nl)

Published by Copernicus Publications on behalf of the European Geosciences Union.

Abstract

With the aim to establish and understand morphological changes in response to stream restoration measures, a detailed monitoring plan was implemented in a lowland stream called Lunterse Beek, located in the Netherlands. Over a period of 1.5 yr, the monitoring included serial morphological surveys, continuous discharge and water level measurements and riparian vegetation mapping. Morphological processes occurred mainly in the initial period, before riparian vegetation development. In the subsequent period, riparian vegetation started to emerge, with a maximum coverage halfway the survey period, which coincides with the end of the summer period. Detailed morphological and hydrological data show a marked difference in behaviour between the unvegetated initial stage and the vegetated final period. The riparian vegetation cover, obtained from an aerial photo, shows a strong correlation with inundation frequency. We applied linear regression to relate morphological activity to time-averaged bed shear stress. In the initial stage after construction, with negligible riparian vegetation, channel morphology adjusted without a clear response to the discharge hydrograph. In the subsequent period, morphological activity in the channel bed and bank zones showed a clear response to discharge variation. The two stages of morphological response to the restoration measures reveal the role of riparian vegetation, which acts to focus the morphodynamic developments in the main channel.

1 Introduction

Riparian zones play an essential role in restoration of aquatic systems (Naiman and Décamps, 1997). Stream restoration in the Netherlands increasingly often involves the development of riparian zones, along the restored channel reaches. These riparian zones are constructed to accommodate water during flood events, and to improve the connection between aquatic and terrestrial ecology. In this paper we will focus on the effect of riparian vegetation on meander morphodynamics.

Riparian vegetation adds strength to the soil. Root mass is linearly related to soil shear strength, such that even low root densities can provide a substantial increases in shear strength of the soil matrix. Root-reinforced soils are more resistant to deformation and failure than bare soils (Abernethy and Rutherfurd, 2001). The stabilizing effect of riparian vegetation has an impact on meandering of rivers and streams at various spatial scales. The importance of riparian vegetation in contributing to channel bank stability is widely recognized (e.g. Simon and Collison, 2002; Pollen-Bankhead and Simon, 2009). The mechanical effect of riparian vegetation causes an increase of bank stability, through the increase of tensile strength of the soil. On the other hand, hydrological processes (i.e. interception and transpiration by vegetation) could cause a decrease of bank stability, e.g. through an increase of pore-water pressure due to higher infiltration through macropores (Simon and Collison, 2002).

River meandering processes may induce differences in riparian vegetation biomass density (Perucca et al., 2006). Perucca et al. (2007) constructed a process-based vegetation model, coupled with a fluid dynamics model. Their results show that riparian vegetation is potentially responsible for changes in meander planform characteristics, including wavelength and skewness. On a reach scale, riparian vegetation affects channel patterns. Recently, laboratory experiments have shown how riparian vegetation may stabilize floodplain material, causing initial braided channel patterns to shift towards single-thread (meandering) channels (Gran and Paola, 2001; Braudrick et al., 2009; Tal and Paola, 2010). Van de Wiel and Darby (2004) studied morphological developments at the reach-scale in a numerical model. They showed that riparian vegetation density and root structure were the most influential parameters controlling reach-scale morphodynamics.

Details of hydrological disturbances, i.e. the duration, intensity, frequency and extent of floods, include the most important factors influencing riparian vegetation development (Merritt et al., 2010). Biological and chemical processes form secondary controls on species presence and abundance (Gurnell et al., 2012). The influence of these hydrological disturbances on riparian vegetation is most apparent in lowland areas, where

floodplains are typically broad and flat. In these areas, species-specific responses to hydrological disturbances are related to soil moisture/oxygenation, sediment deposition, the frequency and duration of inundation, and the erosive action of flooding (Ward et al., 2002). Each riparian species has a different tolerance and growth response to hydrological disturbances (Gurnell et al., 2012). These differences affect the spatial distribution of species according to topography, sediment texture and landform stability within the riparian zone, both in lateral (e.g. Johnson et al., 1995; Naiman et al., 2005) and longitudinal direction (e.g. Bertoldi et al., 2011). In a stochastic model study, Camporeale and Ridolfi (2006) showed how random variation in river discharges results in lateral variability of the distribution of riparian vegetation. Camporeale and Ridolfi (2010) extended this model with a physically-based morphodynamic model (Zolezzi and Seminara, 2001). They showed that active meander processes affect the development of riparian vegetation, especially in high-curvature bends. This paper zooms into a low-energy stream environment, showing how riparian vegetation reduces the morphodynamic developments that occur in an initial, unvegetated stage after construction of the channel.

Serial digital elevation models (DEMs) offer the opportunity to quantify morphological change on the reach scale. Several survey techniques have been used to collect topographic data for DEM construction in fluvial environments, e.g. a total station (Fuller et al., 2003), ground-based GPS (Brasington et al., 2003), photogrammetry (Lane et al., 2010), Terrestrial Laser Scanning (TLS) (Wheaton et al., 2013) and airborne LiDAR (Croke et al., 2013). Temporal morphological changes could be detected when a study reach is surveyed more than once. A DEM of Difference (DoD) may quantify these changes when comparing two serial DEMs (Lane et al., 2003). DoD in braided rivers have been extensively applied on reach-scale (e.g. Lane et al., 2010; Wheaton et al., 2010b, 2013). DoD analysis in meandering rivers is often restricted to bend-scale (e.g. Gautier et al., 2010; Kasvi et al., 2013), although there are several exceptions in meandering rivers (Fuller et al., 2003; Erwin et al., 2012; Croke et al., 2013). Until now, these studies are typically based on annual (e.g. Wheaton et al., 2013) or bi-annual surveys

(Fuller et al., 2003; Lane et al., 2010). This low temporal resolution can cause erosional and depositional patches to overlap, complicating sediment budget estimation. Besides sediment budget estimation, DoD analysis has been used to relate individual erosional and depositional patches to morphological and ecological processes (e.g. Grove et al., 2013; Wheaton et al., 2010a), often called DoD segregation.

Here we present a field study based on 13 high-resolution surveys over a period of 1.5 yr, where we combined morphological and terrestrial ecological data, under varying discharge conditions. The objective is to establish and understand the morphological response of a lowland stream to riparian vegetation development and varying discharge conditions.

2 Study area

In October 2011 a stream restoration project was realized in a small lowland stream, the Lunterse Beek, located in the central part of the Netherlands (52°4′46″ N, 5°32′30″ E), see Fig. 1. A canalized channel was replaced by a channel with a sinuous planform. The course of the new channel crosses the former channel at several locations (Fig. 1c). The channel was constructed with a width of 6 m, a depth of 0.4 m and a longitudinal slope of 1.1 m km^{-1}. A lowered floodplain surrounded the channel, with an average width of 20 m, see Fig. 1d. The bed material mainly consists of fine sand, with a median grain size of 218 µm (Eekhout and Hoitink, in review).

Figure 1b shows the location of the study area in the catchment. The catchment has an area of 63.6 km^2. The elevation within the catchment varies between 3 to 25 m above mean sea level. The study area is located in a mildly sloping area. The subsurface of the catchment mainly consists of drifting sand deposits. The average yearly precipitation amounts to 796 mm yr^{-1}. The average daily discharge amounts to 0.33 m^3 s^{-1} and the peak discharge during the study period was 6.46 m^3 s^{-1}.

A chute cutoff occurred within 3 months after realization of the stream restoration project, which has been studied in Eekhout and Hoitink (in review). Prior to the cutoff,

a plug bar was deposited in the bend to be cutoff. Hydrodynamic model results show the location of the plug bar coincides with the region where flow velocity drops below the threshold of sediment motion, indicating the sediment deposition was caused by a backwater effect. Upstream from the plug bar, an embayment formed in the floodplain at a location where the former channel was located. The former channel was filled with sediment prior to channel construction. It is likely that the sediment at this location was less consolidated, and therefore, was prone to erosion. The chute channel continued to incise and to widen into the floodplain and, after 6 months, acted as the main channel, conveying the discharge during the majority of time.

3 Material and methods

3.1 Morphological monitoring

The temporal evolution of the bathymetry has been monitored over a period of 1.5 yr. Morphological data were collected in the area within the lowered floodplain over a length of 180 m, indicated by light grey in Fig. 1d. Morphological data were collected with an average frequency of 45 days, using RTK-GPS equipment (Leica GPS 1200+) to measure surface elevation with an accuracy between 1 and 2 cm. The surface elevation data were collected along cross-sections between the two floodplain edges. We followed the survey strategy proposed by Milan et al. (2011), focusing on breaks of slope. We increased the point-density in the vicinity of steep slopes (e.g. channel banks), and decreased the point-density on flat surfaces (e.g. floodplains).

3.2 DEM construction and processing

Digital Elevation Models (DEMs) of each of the thirteen datasets were constructed. The data were transformed to s, n-coordinates using the method described by Legleiter and Kyriakidis (2007). Since the data were collected in cross-sections, an anisotropy

factor was used within the interpolation routine, accounting for dispersion of the collected data in the longitudinal direction. We determined the anisotropy factor by dividing the average streamwise distance between the subsequent cross-sections by the average cross-stream distance between the individual point measurements. The data were split into a channel section and a floodplain section, to account for a higher density of point measurements in the channel than in the floodplain. We applied a separate anisotropy factor for the channel and the floodplain data. Table 1 lists the point density and anisotropy factors for all individual surveys, specified for the channel and floodplain sections.

We projected the data onto a curvilinear grid, following the channel centerline for the channel data and the valley centerline for the floodplain data. A Triangular Irregular Netwerk (TIN) was constructed using a Delaunay triangulation routine in Matlab, following Heritage et al. (2009). Subsequently, the TIN was interpolated onto a grid using nearest neighbour interpolation, with a grid spacing of 0.25 m. After interpolation, the data were transformed back to x, y-coordinates. The interpolated channel and floodplain were then merged to facilitate the comparison between all thirteen surveys.

Deposition and erosion patterns were obtained by subtracting two subsequent morphological surveys, yielding a DoD. Real morphological change can be different from apparent morphological change, which may arise from uncertainties in the individual DEMs, e.g. from instrumental errors or errors that arise from the interpolation routine. The uncertainty can be established by determining the threshold level of detection (LoD). We adopted the method by Milan et al. (2011) to construct the spatially distributed LoD. Milan et al. (2011) account for the increase of spatially distributed error in a DEM near steep surfaces (e.g. channel bank edges), by inferring the relationship between the standard deviation of elevation errors and local topographic roughness. We adjusted the method by Milan et al. (2011), by adopting a single linear regression model to obtain the spatial standard deviation of elevation error grids. The regression model was obtained after combining elevation errors and local topographic roughness values (Fig. 2a), for all 13 surveys.

We obtained the LoD in each grid cell according to:

$$U_{\text{crit}} = t\sqrt{(\sigma_{\text{e1}})^2 + (\sigma_{\text{e2}})^2} \quad (1)$$

where U_{crit} is the critical threshold error, t is the critical student's value and σ_{e1} and σ_{e2} are the standard deviation of elevation error, for the first and second survey, respectively. The threshold value is based on a critical student's t value, at a chosen confidence level. Following Milan et al. (2011), we applied a confidence limit equal to 95 %, which results in $t \geq 1.96$ (2σ). The elevation difference between two subsequent surveys at a particular grid cell is insignificant when $z_{i,j}(\text{new}) - z_{i,j}(\text{old}) < U_{\text{crit}}$, where $z_{i,j}(\text{new})$ and $z_{i,j}(\text{old})$ are the elevations of the two subsequent morphological surveys at a particular grid cell. We adopted a lower bound for the critical threshold error, to account for the accuracy of the RTK-GPS equipment. This lower bound was set to $U_{\text{crit}} = 0.04$ m, which is 2 times the maximum error in the measurements.

Morphological activity was quantified for the study area as a whole, and for isolated geomorphic zones. We segregated the study area into four geomorphic zones: channel bank, channel bed, floodplain and cutoff channel. Figure 3a shows an example of the distribution of each of the four geomorphic zones in the study area, for period (4–5), day 191–231. Segregation of each of the four geomorphic zones was accomplished as follows. The channel bank mask is defined as the zone between the channel bank lines of two subsequent surveys, plus a strip of 0.5 m width on either side of the zone. The channel bed mask is defined as the zone between the two channel bank masks. The remainder of the grid domain is labelled as floodplain, with the cutoff channel considered as a separate geomorphic zone. Finally, we attributed each of the patches of morphological change to one of the geomorphic features (Fig. 3b).

We applied two methods to quantify morphological activity. First, we determined the volumetric change in sediment storage. Volumetric change in sediment storage was determined by multiplying the elevation change by the grid cell area, separated in gross erosion and gross deposition. We determined net sediment change by subtracting gross erosion from gross deposition. Second, we determined the root-mean-square

elevation difference:

$$\mathrm{RMSD} = \sqrt{\sum (z_{i,j}(\mathrm{new}) - z_{i,j}(\mathrm{old}))^2} \quad (2)$$

Where $z_{i,j}$ is the elevation in grid cell i, j of the DEM. The volumetric change in sediment storage and the root-mean-square elevation difference were expressed as a rate of change, by dividing both quantities by the time between two successive surveys.

3.3 Hydrological monitoring

Discharge data were collected downstream of the study reach at a discharge measurement weir, indicated with Q in Fig. 1c. Discharge estimates were acquired with a one-hour frequency. Water level data were collected at a water level gauge in the study area, indicated with WL1 in Fig. 1d. The water level gauge started monitoring 103 days after construction of the channel. The water level gauge was accidentally placed in the cutoff channel. After day 288, the water level gauge was moved to a new location, on the other side of the floodplain, indicated with WL2 in Fig. 1d. Water level data were acquired with a one-hour frequency. Longitudinal water level profiles were measured with RTK-GPS equipment during twelve of the thirteen morphological surveys.

Water level time series and an averaged water level slope were used to determine the inundation frequency in each of the grid cells. The average longitudinal water level slope was calculated from the ten last water level profiles from the GPS surveys, excluding the two pre-cutoff water level profiles. We obtained an average water level slope of 0.49 m km^{-1}. We interpolated daily-averaged water level time series over the entire length and width of the study domain, using the average water level slope. A cell is considered inundated when the difference between the interpolated water level exceeds the surface elevation, obtained from the DEM.

3.4 Riparian vegetation

The restored stream was constructed in bare soil. Riparian vegetation started to develop halfway the study period. The spatial distribution of the riparian vegetation was obtained from an aerial photo (Fig. 4a). The aerial photo shows riparian vegetation has mainly developed in the floodplain. The aerial survey also includes a Colourized Infra-Red (CIR) image (Fig. 4b), which contains data from the Near Infra-Red (NIR) wavelengths (0.78–3 µm). With these data the riparian vegetation development at day 289 is quantified with the Normalized Difference Vegetation Index (NDVI):

$$\mathrm{NDVI} = \frac{\mathrm{NIR} - \mathrm{VIS}}{\mathrm{NIR} + \mathrm{VIS}} \quad (3)$$

where NIR is the intensity of the Near Infra-Red wavelengths and VIS is the intensity of the VISible red wavelengths. Eq. (2) was applied to the entire image, which allowed us to obtain the spatial variation of the NDVI within the study area. NDVI varies between −1.0 and 1.0. Positive values generally correspond to vegetation, whereas negative values correspond to water, or other media that adsorb the infra-red wavelengths (Clevers, 1988).

Figure 4c shows the NDVI for the study area and surrounding agricultural fields and roads. The panel clearly shows positive values for the pasture area on the north-side of the study area. Negative values are obtained inside the channel and on the road, on the south-side of the study area.

3.5 Linear regression modelling

To investigate the degree in which morphological activity is in response to discharge variation, values of the RMSD were related to time-averaged bed shear stress τ (N m^{-2}). Bed shear stress is defined as:

$$\tau(t) = \rho g S R(t) \quad (4)$$

where $\rho = 1000\,\mathrm{kg\,m^{-3}}$ the density of water, $g = 9.81\,\mathrm{m\,s^{-2}}$ is the gravitational acceleration, S is the longitudinal water level slope, $R(t)$ is the hydraulic radius. We used the average longitudinal water level slope S as described earlier. The hydraulic radius $R(t)$ was obtained by dividing the cross-sectional flow area $A(t)$ by the wetted perimeter $P(t)$, obtained from the cross-section at the location of the water level gauge. We applied Eq. (4) to the discharge and water level time series and averaged between two successive morphological surveys, to obtain an estimate of the time-averaged bed shear stress per period.

Linear regression models were determined, relating the RMSD to time-averaged bed shear stress, for the study area as a whole and for each of the four geomorphic zones separately. Linear regression models were determined for the vegetated period (5–13) only. We tested the hypothesis that morphological activity in the unvegetated period was significantly different from the vegetated period. We determined the 95 %-confidence intervals based on the t-distribution, with the degrees of freedom corresponding to the number of vegetated periods.

4 Results and discussion

4.1 Morphodynamics

Figures 5 and 6 show the DEMs and DoDs of the thirteen morphological surveys, respectively. The first three surveys (day 0, 93 and 133) show the sequence of morphological changes that capture the chute cutoff event. The first DoD (day 0–93) shows deposition of sediment on the channel bed, which is associated with the formation of a plug bar (Eekhout and Hoitink, in review). An initial embayment had formed upstream from the bend to be cutoff. The actual cutoff occurred in the second period (day 93–133), where a new channel incised into the floodplain. In the subsequent period (day 133–231), the morphological changes occurred mainly in the bend at the downstream end of the study area. During this period, in this bend we observed both erosion of

the outer bank and accretion in the inner bank. Maximum bank erosion amounted to 2.5 m between day 133 and 191 (2.6 channel widths per year). Subsequently, there was a period of little morphological change (day 231–288). In the last period (day 341–558), morphological changes were restricted to the channel bed and banks. Maximum bank erosion amounted to 0.7 m between day 341 and 377 (1.2 channel widths per year). At that time, little morphological change was observed in the floodplain.

Overall, dynamics of the bed level is highest in the downstream half of the study area. Figure 5 clearly illustrates the channel bed incision of the bend at the downstream end of the study area, in the period following the chute cutoff. The upstream half of the study area did not show pronounced morphological changes. Apart from occasional changes in the channel bed, no structural bank erosion or accretion was observed.

Figure 7 shows the sediment budget, which we derived from the DoDs (Fig. 6). Figure 7a shows volumetric change over the study area as a whole, aggregated for regions of erosion and deposition, and net change. Figure 7b shows the volumetric change, subdivided per geomorphic zone. Considering the study area as a whole (Fig. 7a), a shift from net deposition to net erosion is observed. In the first period (1–2), deposition is mainly caused by the deposition of sediment in the channel bed, including the cutoff channel. This is followed by a period (2–4) of limited net change, where bank erosion is balanced by net deposition in the rest of the study area. From the fifth survey onwards, the sediment balance shifts towards net erosion. Channel bed processes (channel incision) are the dominant contributor to the net erosion of sediment in the study area.

4.2 Riparian vegetation development

Figure 8a shows the positive values of the NDVI in the study area, indicating the extent of the riparian vegetation at day 289. Riparian vegetation did not develop uniformly over the floodplain. Riparian vegetation cover (observed as a positive NDVI-value) amounted to 53 % of the study area. At the time of the aerial photograph, riparian vegetation covered 34 % of the channel bank zone, 3 % of the channel bed zone, 79 %

of the floodplain zone, and 59 % of the cutoff channel zone. This shows riparian vegetation did not develop as abundantly in the cutoff channel as in the rest of the floodplain. There is also a clear distinction between channel (bed and bank) and floodplain.

The inundation frequency for each of the cells covering the study area clearly shows the distinction between channel and floodplain, with inundation in the channel areas occurring more frequently (Fig. 8b). The cutoff channel also inundates more frequently than the floodplain. The average inundation frequency was 56 % in the channel bank zone, 95 % in the channel bed zone, 32 % in the floodplain zone, and 77 % in the cutoff channel zone. A comparison of the inundation percentages to the riparian vegetation percentages shows riparian vegetation cover decreases with increasing inundation frequency.

We divided the inundation frequency into classes of 5 % and determined the riparian vegetation cover per inundation class, relating Fig. 8a to 8b. Figure 8c shows that riparian vegetation cover decreases with increasing inundation frequency. The riparian vegetation cover has a maximum around 85 % in areas where inundation frequency is less than 55 %. With increasing inundation frequency, riparian vegetation cover gradually decreases towards 8 % for areas inundating between 95 % and 100 % of the time.

Figure 9 shows the series of twelve oblique terrestrial photos taken from the location indicated in Fig. 1d. Just after construction had finished at day 0 (first photo of row one), riparian vegetation was visible on the left channel bank. In general, riparian vegetation was absent in the floodplain. In the subsequent period, until day 161 (third photo of row one), no change in riparian vegetation coverage was observed. Riparian vegetation started to develop around day 231 (last photo of row one). Some patches of riparian vegetation are emerging in the floodplain and at the channel banks. The development of riparian vegetation continued in the following period and a maximum riparian vegetation coverage was observed at day 341 (second photo of row two). At that moment, the floodplain was almost entirely covered with riparian vegetation. Only in the cutoff channel, riparian vegetation did not develop as abundantly as in the floodplain. In the period until the end of the study period, from day 377 (third photo of row

two) until day 558 (the last photo of row four), the riparian vegetation cover started to decrease, approximately to a level similar to the situation between day 231 and 288.

4.3 Morphodynamic regime change

Figure 10a shows morphological change ($m\,yr^{-1}$), which has been derived from Fig. 6, with Eq. (2). Figure 10b shows the discharge hydrograph, obtained from the measurement weir located 360 m downstream from the study area. The temporal evolution of the morphological change (black diamonds in Fig. 10a) shows that the RMSD metric of morphological change was relatively high in the first two periods (1–3). In the subsequent period, morphological changes show a decreasing trend until period (6–7). In the final period, incidental peaks are observed during periods of increased discharges, i.e. in period (7–8) and (9–10).

From Fig. 10a it appears that the study period can be divided into two stages. The first stage can be considered an apparent morphological disequilibrium. The interval between surveys 1 and 3 is largely dominated by the chute cutoff event, which is followed by an interval until survey 5 that is dominated by channel bank processes. The second stage can be considered to be a morphodynamic equilibrium, in the sense the reach-scale morphology has stabilized. Both channel bank and channel bed processes dominate morphological change in the latter stage. During the whole study period, morphological changes in the floodplain contributed only slightly to the overall changes in the study area.

The temporal development of riparian vegetation, indicated with the green shaded colours in Fig. 10, shows reach-scale riparian vegetation development from day 231 onwards. A maximum riparian vegetation coverage is observed in period (7–8), which corresponds with the photo taken on day 341 (Fig. 9, second photo on row two). In the subsequent period, until the end of the study period, a decrease of riparian vegetation cover is observed. In Fig. 10b, two periods of extremely high discharges occurred, i.e. in period (1–2) and period (9–10), which can be associated with prolonged periods of precipitation. In other periods, accidental peaks in discharge are associated with high-

intensity precipitation events, which commonly result in peak discharges in regulated lowland catchments.

Figure 10 shows that in the stage of morphological disequilibrium, rates of morphological change are relatively high, without showing a clear response to discharge variation. In the subsequent equilibrium stage, a clear response to the varying discharge is evident. Figure 9 shows that riparian vegetation was virtually absent in periods (1–5), after which riparian vegetation started to develop in the entire study area. The difference in morphological behaviour in the two stages of development indicates riparian vegetation can have a substantial influence on time that elapses before an equilibrium is reached.

Figure 11 shows the results from the linear regression between RMSD and time-averaged bed shear stress. The five regression models show differences in slope, where a steeper slope corresponds to a stronger response. The strongest response is found for the channel bed and the weakest for the floodplain. This is reflected in the model performance, with a higher coefficient of determination for the channel bed and a lower for the floodplain.

The RMSD in a certain period is significantly different from the linear regression model when the value is outside the 95 %-confidence interval (95 %-CI). Considering the study area as a whole, the entire unvegetated period is outside the 95 %-CI. This reveals the morphodynamic behaviour during the unvegetated period is significantly different from the vegetated period. This is mainly caused by the morphological response observed in the channel bank and cutoff channel zones (Fig. 11b and e). In the channel bank zone the morphological response is outside the 95 %-CI in periods (2–5) and in the cutoff channel zone in periods (1–5). The channel bank processes that occurred in these periods may be related to the absence of channel bank vegetation, causing an increase of bank processes, i.e. bank erosion and accretion. In the channel bed and floodplain zones, none of the unvegetated periods are outside the 95 %-CI. Riparian vegetation developed only in a small percentage of the channel bed zone (3 % cover). This explains why the morphological activity does not show an apparent

response to the development of riparian vegetation. Riparian vegetation covered 79 % of the floodplain zone, however, morphological activity in this zone is not affected by the riparian vegetation development. In general, only limited morphological activity is observed in the floodplain.

From Fig. 11 it appears that morphological activity in the unvegetated period is significantly different from the vegetated period. Figure 6 shows that active meander processes occurred in the initial unvegetated periods, i.e. the occurrence of a chute cutoff and bank erosion and accretion. In the following period, when riparian vegetation started to emerge, these active meander processes were less pronounced, although localized bank erosion can be observed. The morphodynamic regime change shows similarities with laboratory experiments where riparian vegetation caused a transition from an initially braided channel pattern towards a stable single-thread channel (Gran and Paola, 2001; Braudrick et al., 2009; Tal and Paola, 2010). Both our observations and the findings from these laboratory experiments show that riparian vegetation can cause a shift from a high-energy channel pattern (e.g. braided or meandering with chutes), towards a low-energy channel pattern, such as a meandering or a laterally immobile single-thread channel.

A regime change from an initial unvegetated stage, in which the reach-scale morphology adjusts towards a dynamic equilibrium, and a subsequent vegetated stage, where morphodynamic changes are concentrated in the channel bed zone, can be a general phenomenon in lowland stream restoration projects. Within these projects, it may be worthwhile to minimize the duration of the initial stage of morphological adaptations. To some extent this duration can be manipulated by changing the seasonal timing of the construction of the channel, which has an impact on the duration of the pre-vegetation period. Once the reach-scale topography is known, the initial riparian vegetation cover could be predicted, based on inundation frequency.

5 Conclusions

A detailed monitoring plan was implemented to monitor a restored lowland stream for a period of 1.5 yr after channel construction. We combined morphological, hydrological and ecological data to establish interactions between reach-scale morphodynamics, discharge dynamics and riparian vegetation development. In the initial stage after channel construction, when negligible riparian vegetation was present, channel morphology adjusted rapidly towards an alternative, complex topography. Maximum bank erosion rates amounted to 2.6 channel widths per year. In the subsequent stage riparian vegetation emerged. The spatial distribution of the riparian vegetation is found to be governed by inundation frequency. Channel bed incision and localized bank erosion dominate the morphodynamic developments after riparian vegetation developed, with maximum bank erosion rates amounting to 1.2 channel widths per year. Linear regression analysis shows that the morphological response to bed shear stress is significantly different between the unvegetated and vegetated stages. The two stages of morphological adjustments after the restoration measures reveal how riparian vegetation causes a morphodynamic regime change, which may be a general phenomenon in lowland stream restoration projects.

Acknowledgements. This study is part of a research project (Beekdalbreed Hermeanderen) funded by Agency NL (project code KRW 09023). We thank Philip Wenting (Wageningen University) for his contribution to the fieldwork campaign, and Paul Torfs (Wageningen University) for his help in post-processing of field data. We thank Slagboom en Peeters Luchtfotografie B.V. for providing the aerial photo. Also, we thank Remko Uijlenhoet (Wageningen University), Piet Verdonschot (Alterra), Rob Fraaije (Utrecht University) and Christian Huising (Waterschap Vallei en Veluwe) for their comments on the draft manuscript.

References

Abernethy, B. and Rutherfurd, I. D.: The distribution and strength of riparian tree roots in relation to riverbank reinforcement, Hydrol. Process., 15, 63–79, 2001. 713

Bertoldi, W., Drake, N. A., and Gurnell, A. M.: Interactions between river flows and colonizing vegetation on a braided river: exploring spatial and temporal dynamics in riparian vegetation cover using satellite data, Earth Surf. Proc. Land., 36, 1474–1486, doi:10.1002/esp.2166, 2011. 714

Brasington, J., Langham, J., and Rumsby, B.: Methodological sensitivity of morphometric estimates of coarse fluvial sediment transport, Geomorphology, 53, 299–316, doi:10.1016/S0169-555X(02)00320-3, 2003. 714

Braudrick, C. A., Dietrich, W. E., Leverich, G. T., and Sklar, L. S.: Experimental evidence for the conditions necessary to sustain meandering in coarse-bedded rivers, P. Natl. Acad. Sci. USA, 106, 16936–16941, doi:10.1073/pnas.0909417106, 2009. 713, 726

Camporeale, C. and Ridolfi, L.: Riparian vegetation distribution induced by river flow variability: a stochastic approach, Water Resour. Res., 42, W10415, doi:10.1029/2006WR004933, 2006. 714

Camporeale, C. and Ridolfi, L.: Interplay among river meandering, discharge stochasticity and riparian vegetation, J. Hydrol., 382, 138–144, doi:10.1016/j.jhydrol.2009.12.024, 2010. 714

Clevers, J. G. P. W.: The derivation of a simplified reflectance model for the estimation of leaf area index, Remote Sens. Environ., 25, 53–69, 1988. 720

Croke, J., Todd, P., Thompson, C., Watson, F., Denham, R., and Khanal, G.: The use ofmulti temporal LiDAR to assess basin-scale erosion and deposition following the catastrophic January 2011 Lockyer flood, SE Queensland, Australia, Geomorphology, 184, 111–126, doi:10.1016/j.geomorph.2012.11.023, 2013. 714

Eekhout, J. P. C. and Hoitink, A. J. F.: Importance of backwater effects and floodplain heterogeneity in the occurrence of a chute cutoff, J. Geophys. Res., in review, 2013. 715, 721

Erwin, S. O., Schmidt, J. C., Wheaton, J. M., and Wilcock, P. R.: Closing a sediment budget for a reconfigured reach of the Provo River, Utah, United States, Water Resour. Res., 48, W10512, doi:10.1029/2011WR011035, 2012. 714

Fuller, I. C., Large, A. R. G., and Milan, D. J.: Quantifying channel development and sediment transfer following chute cutoff in a wandering gravel-bed river, Geomorphology, 54, 307–323, doi:10.1016/S0169-555X(02)00374-4, 2003. 714, 715

Gautier, E., Brunstain, D., Vauchel, P., Jouanneau, J., Roulet, M., Garcia, C., Guyol, J., and Castro, M.: Channel and floodplain sediment dynamics in a reach of the tropical meandering Rio Beni (Bolivian Amazonia), Earth Surf. Proc. Land., 35, 1838–1853, doi:10.1002/esp.2065, 2010. 714

Gran, K. and Paola, C.: Riparian vegetation controls on braided stream dynamics, Water Resour. Res., 37, 3275–3284, doi:10.1029/2000WR000203, 2001. 713, 726

Grove, J., Croke, J., and Thompson, C.: Quantifying different riverbank erosion processes during an extreme flood event, Earth Surf. Proc. Land., 38, 1393–1406, doi:10.1002/esp.3386, 2013. 715

Gurnell, A. M., Bertoldi, W., and Corenblit, D.: Changing river channels: the roles of hydrological processes, plants and pioneer fluvial landforms in humid temperate, mixed load, gravel bed rivers, Earth-Sci. Rev., 111, 129–141, doi:10.1016/j.earscirev.2011.11.005, 2012. 713, 714

Heritage, G. L., Milan, D. J., Large, A. R. G., and Fuller, I. C.: Influence of survey strategy and interpolation model on DEM quality, Geomorphology, 112, 334–344, doi:10.1016/j.geomorph.2009.06.024, 2009. 717

Johnson, W. C., Dixon, M. D., Simons, R., Jenson, S., and Larson, K.: Mapping the response of riparian vegetation to possible flow reductions in the Snake River, Idaho, Geomorphology, 13, 159–173, 1995. 714

Kasvi, E., Vaaja, M., Alho, P., Hyyppä, J., Kaartinen, H., and Kukko, A.: Morphological changes on meander point bars associated with flow structure at different discharges, Earth Surf. Proc. Land., 38, 577–590, doi:10.1002/esp.3303, 2013. 714

Lane, S. N., Westaway, R. M., and Hicks, D. M.: Estimation of erosion and deposition volumes in a large, gravel-bed, braided river using synoptic remote sensing, Earth Surf. Proc. Land., 28, 249–271, doi:10.1002/esp.483, 2003. 714

Lane, S. N., Widdison, P. E., Thomas, R. E. ans Ashworth, P. J., Best, J. L., Lunt, I. A., Sambrook Smith, G. H., and Simpson, C. J.: Quantification of braided river channel change using archival digital image analysis, Earth Surf. Proc. Land., 35, 971–985, doi:10.1002/esp.2015, 2010. 714, 715

Legleiter, C. J. and Kyriakidis, P. C.: Forward and inverse transformations between cartesian and channel-fitted coordinate systems for meandering rivers, Math. Geol., 38, 927–958, doi:10.1007/s11004-006-9056-6, 2007. 716

Merritt, D. M., Scott, M. L., Poff, N. L., Auble, G. T., and Lytle, D. A.: Theory, methods and tools for determining environmental flows for riparian vegetation: riparian vegetation-flow response guilds, Freshwater Biol., 55, 206–225, doi:10.1111/j.1365-2427.2009.02206.x, 2010. 713

Milan, D. J., Heritage, G. L., Large, A. R. G., and Fuller, I. C.: Filtering spatial error from DEMs: implications for morphological change estimation, Geomorphology, 125, 160–171, doi:10.1016/j.geomorph.2010.09.012, 2011. 716, 717, 718

Naiman, R. J. and Décamps, H.: The ecology of interfaces: riparian zones, Annu. Rev. Ecol. Syst., 28, 621–658, 1997. 712

Naiman, R. J., Decamps, H., and McClain, M. E.: Riparia, Elsevier, 2005. 714

Perucca, E., Camporeale, C., and Ridolfi, L.: Influence of river meandering dynamics on riparian vegetatin pattern formation, J. Geophys. Res., 111, G01001, doi:10.1029/2005JG000073, 2006. 713

Perucca, E., Camporeale, C., and Ridolfi, L.: Significance of the riparian vegetation dynamics on meandering river morphodynamics, Water Resour. Res., 43, W03430, doi:10.1029/2006WR005234, 2007. 713

Pollen-Bankhead, N. and Simon, A.: Enhanced application of root-reinforcement algorithms for bank-stability modeling, Earth Surf. Proc. Land., 34, 471–480, doi:10.1002/esp.1690, 2009. 713

Simon, A. and Collison, A. J. C.: Quantifying the mechanical and hydrologic effects of riparian vegetation on streambank stability, Earth Surf. Proc. Land., 27, 527–546, doi:10.1002/esp.325, 2002. 713

Tal, M. and Paola, C.: Effects of vegetation on channel morphodynamics: results and insights from laboratory experiments, Earth Surf. Proc. Land., 35, 1014–1028, doi:10.1002/esp.1908, 2010. 713, 726

Van de Wiel, M. J., and Darby, S. E.: Riparian Vegetation and Fluvial Geomorphology, chap. Numerical modeling of bed topography and bank erosion along tree-lined meandering rivers, 267–282, Water Science and Application Series 8, American Geophysical Union, Washington, DC, 2004. 713

Van Heerd, R. M., Kuijlaars, E. A. C., Teeuw, M. P., and 't Zand, R. J. V.: Productspecificatie AHN 2000, Tech. Rep. MDTGM 2000.13, Rijkswaterstaat, Adviesdienst Geo-informatie en ICT, Delft, 2000. 733

Ward, J. V., Tockner, K., Arscott, D. B., and Claret, C.: Riverine landscape diversity, Freshwater Biol., 47, 517–539, doi:10.1046/j.1365-2427.2002.00893.x, 2002. 714

Wheaton, J. M., Brasington, J., Darby, S. E., Merz, J., Pasternack, G. B., Sear, D., and Vericat, D.: Linking geomorphic changes to salmond habitat at a scale relevant to fish, River Res. Appl., 26, 469–486, doi:10.1002/rra.1305, 2010a. 715

Wheaton, J. M., Brasington, J., Darby, S. E., and Sear, D. A.: Accounting for uncertainty in DEMs from repeat topographic surveys: improved sediment budgets, Earth Surf. Proc. Land., 35, 136–156, doi:10.1002/esp.1886, 2010b. 714

Wheaton, J. M., Brasington, J., Darby, S. E., Kasprak, A., Sear, D., and Vericat, D.: Morphodynamic signatures of braiding mechanisms as expressed through change in sediment storage in a gravel-bed river, J. Geophys. Res., 118, 759–779, doi:10.1002/jgrf.20060, 2013. 714

Zolezzi, G. and Seminara, G.: Downstream and upstream influence in river meandering, Part 1: General theory and application to overdeepening, J. Fluid Mech., 438, 183–211, doi:10.1017/S002211200100427X, 2001. 714

Table 1. Overview of all morphological measurements, with point density (PD) and anisotropy factor (AF) as used in the interpolation routine, specified for the channel and floodplain areas.

Survey no.	Survey date (day)	No. data points	PD (all) (points m^{-2})	PD (channel) (points m^{-2})	AF (channel)	PD (floodplain) (points m^{-2})	AF (floodplain)
1	0	379	0.16	0.25	9.74	0.12	4.59
2	93	956	0.32	0.44	5.04	0.24	2.35
3	133	918	0.27	0.34	3.57	0.24	2.15
4	191	742	0.20	0.31	4.24	0.15	2.04
5	231	1158	0.30	0.45	4.19	0.24	2.09
6	288	1376	0.35	0.53	4.42	0.29	2.15
7	341	1296	0.32	0.50	4.04	0.26	1.86
8	377	1655	0.42	0.62	3.56	0.35	1.68
9	426	1484	0.39	0.58	3.50	0.31	1.64
10	454	1472	0.36	0.55	4.12	0.30	2.03
11	489	1420	0.35	0.51	4.08	0.29	2.05
12	525	1462	0.37	0.56	4.66	0.29	2.15
13	558	1256	0.31	0.50	4.08	0.24	1.77

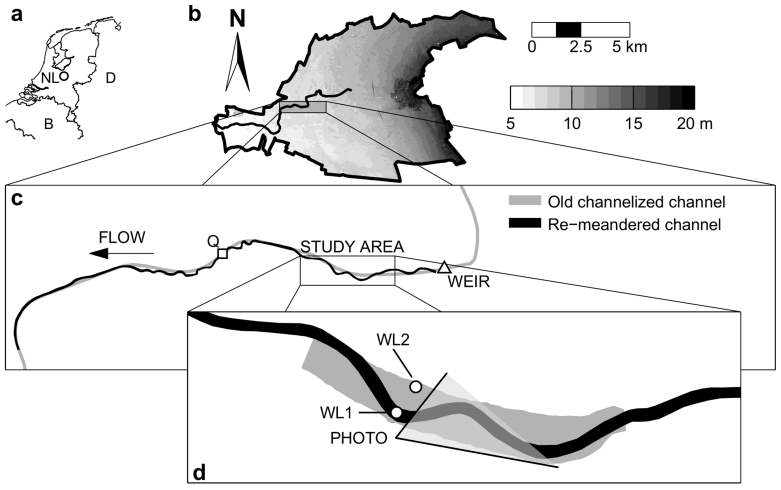

Fig. 1. Overview of the study area: **(a)** location of the study area in the Netherlands, **(b)** elevation model of the catchment (Actueel Hoogtebestand Nederland, AHN; Van Heerd et al., 2000), **(c)** planform of the restored reach, with the squared marker indicating the location of the discharge station (Q), and **(d)** sketch of the study area, indicating the location of the water level gauges (WL1 and WL2) and the approximate extent of available terrestrial photos (grey-shaded triangle, Fig. 9).

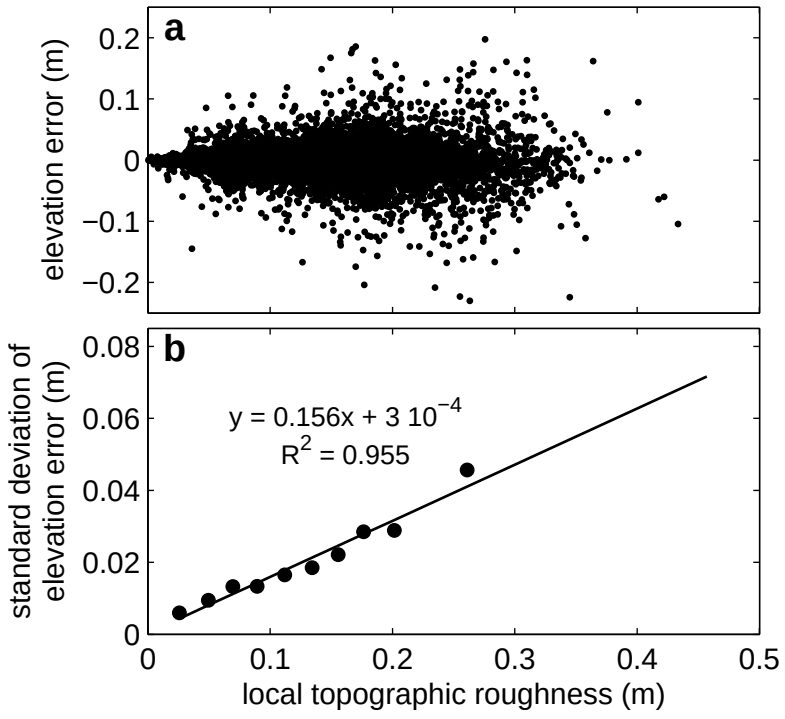

Fig. 2. Variation in elevation errors with local topographic roughness, **(a)** elevation errors for each measured x, y-coordinate for all thirteen surveys, where elevation error increases with increasing local topographic roughness, **(b)** standard deviation of the elevation error for 10 classes of the local roughness. Panel **(b)** also includes the linear regression model and coefficient of determination.

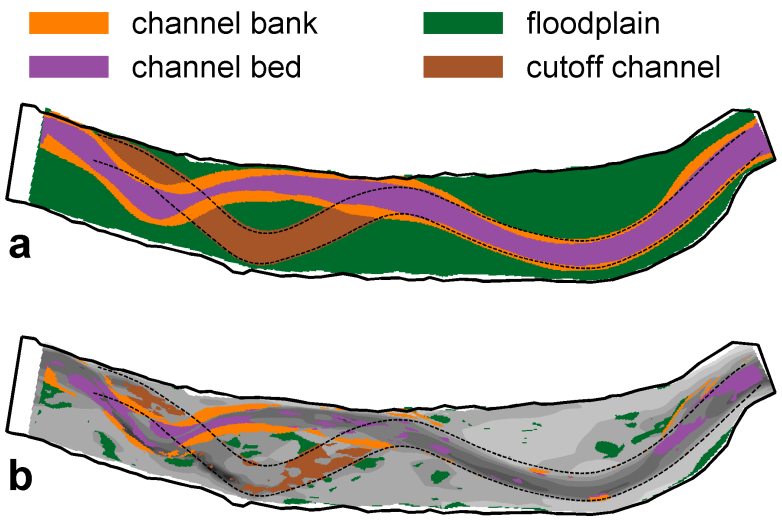

Fig. 3. Segregation of geomorphic zones, for period (4–5), day 191–231. **(a)** Masks of each of the four geomorphic zones, i.e. channel bank (orange), channel bed (purple), floodplain (green) and cutoff channel (brown). **(b)** Resulting segregation of erosional/depositional patches.

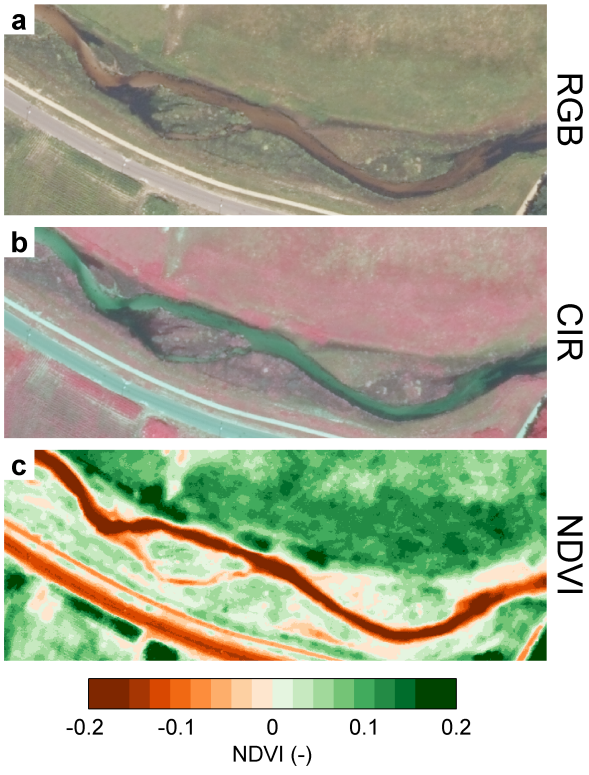

Fig. 4. Aerial photos from which the NDVI was determined, showing **(a)** the RGB-image, **(b)** the CIR-image, and **(c)** the NDVI. In panel **(c)**, the green coloured areas indicate positive NDVI-values and orange coloured areas indicate negative NDVI-values. All images have a 25 cm resolution.

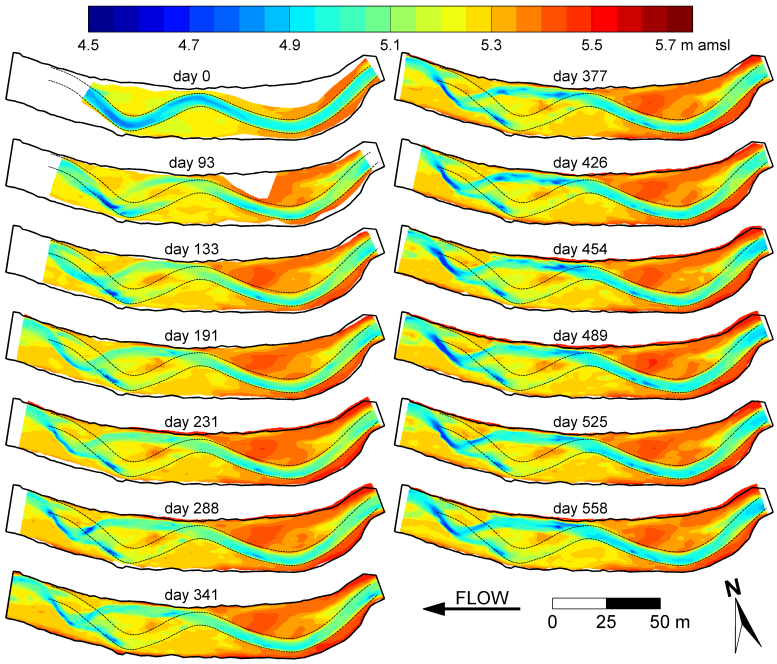

Fig. 5. Digital Elevation Models (DEMs) of all thirteen morphological surveys. The number of days indicates the time since construction of the channel. The dashed black lines indicate the location of the channel banks of the constructed channel. The solid black line surrounding the DEMs indicates the extent of the seventh morphological survey (day 341). Elevation is indicated in meters above mean sea level.

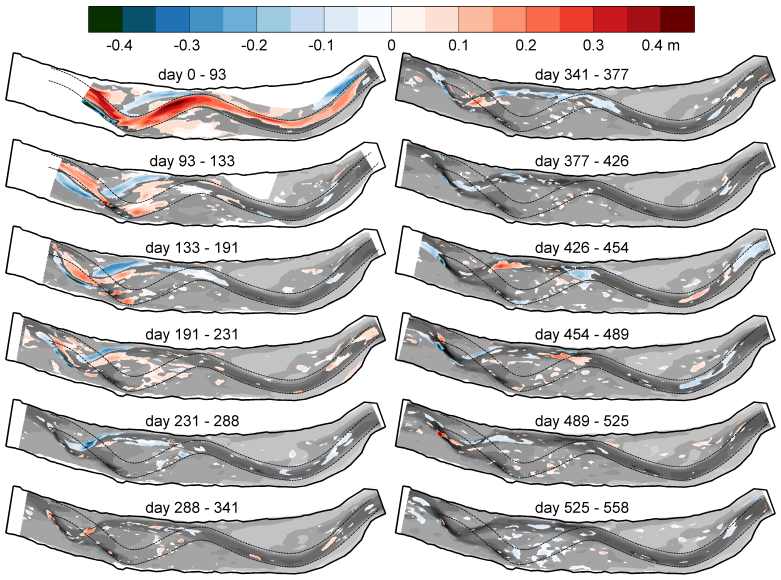

Fig. 6. DEMs of Differences (DoDs) of all twelve periods between the thirteen morphological surveys. The number of days indicates the time since construction of the channel. The dashed black lines indicate the location of the channel banks of the constructed channel. The solid black line surrounding the DEMs indicates the extent of the seventh morphological survey (day 341). Erosion is indicated in blue and deposition in red. The DEM of the first of the two DEMs is shown in grey-scale.

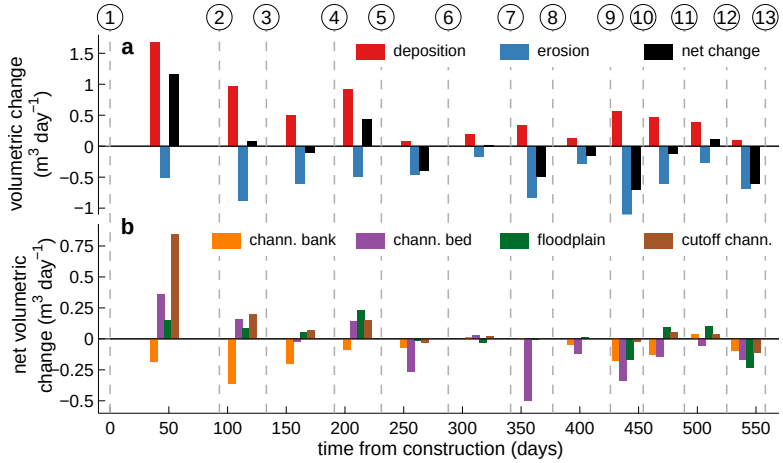

Fig. 7. Temporal evolution of the volumetric change in sediment storage. **(a)** Volumetric change in sediment storage ($m^3\,day^{-1}$), for regions of deposition (red), erosion (blue), and net change (black). **(b)** Volumetric change in sediment storage ($m^3\,day^{-1}$), specified per geomorphic feature, with channel bank (orange), channel bed (purple), floodplain (green), and cutoff channel (brown). The dashed vertical lines indicate the surveying moments, the numbers at the top of the figure correspond with the numbers in Table 1.

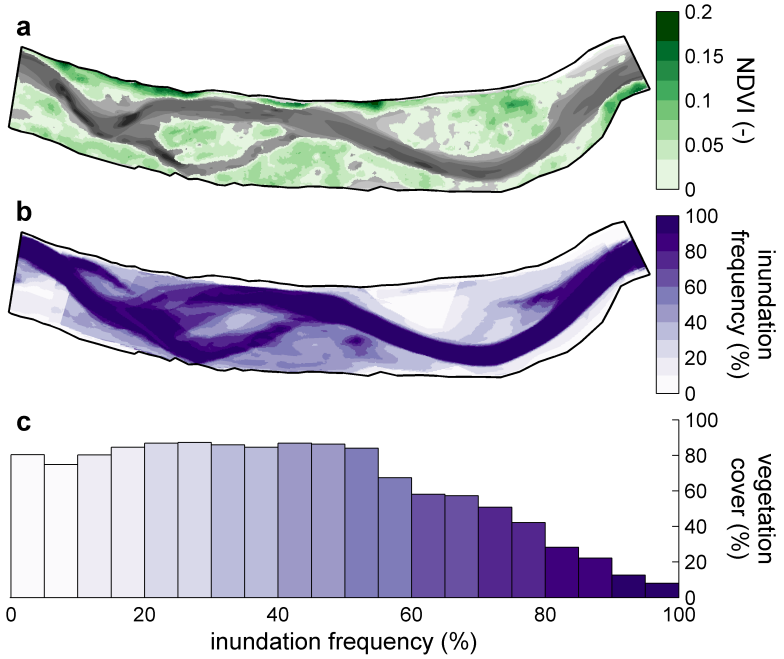

Fig. 8. (a) Extent of riparian vegetation in the study area. **(b)** Spatial variation of the inundation frequency for the time period from the start of the water level measurements (day 104) until the sixth morphological survey (day 288). **(c)** Percentage of riparian vegetation cover per inundation class.

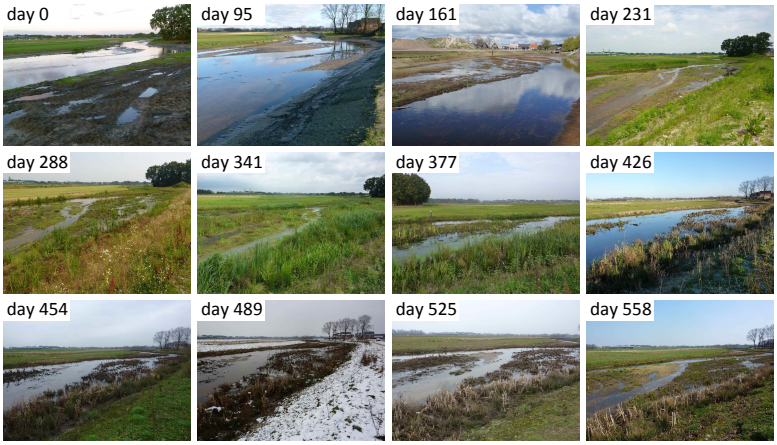

Fig. 9. Series of twelve oblique terrestrial photos taken from the location indicated in Fig. 1d, except for the third photo (day 161), which was taken from the other side of the floodplain.

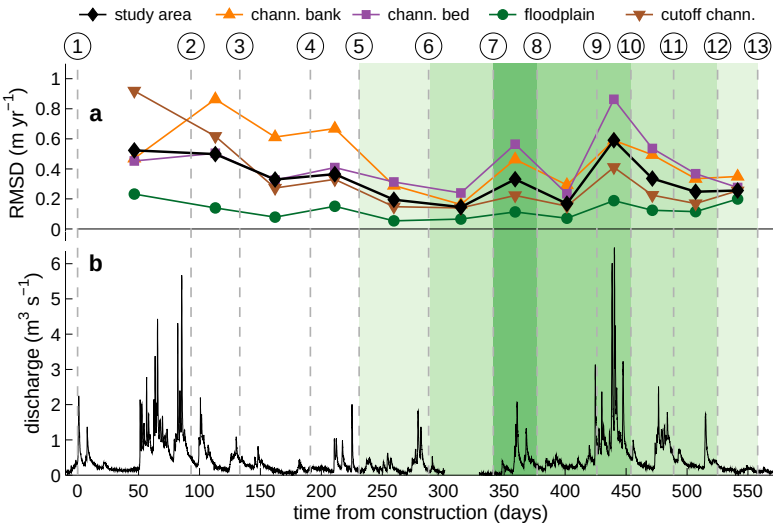

Fig. 10. Temporal evolution of: **(a)** the rate of morphological change (m yr^{-1}) for the study area as a whole (black diamonds), and specified per morphological feature, with channel bank (orange triangles), channel bed (purple squares), floodplain (green circles), and cutoff channel (brown triangles), and **(b)** discharge hydrograph (m^3 s^{-1}). The green shaded colours indicate the riparian vegetation coverage, estimated from Fig. 9. The dashed vertical lines indicate the surveying moments, the numbers at the top of the figure correspond to the numbers in Table 1.

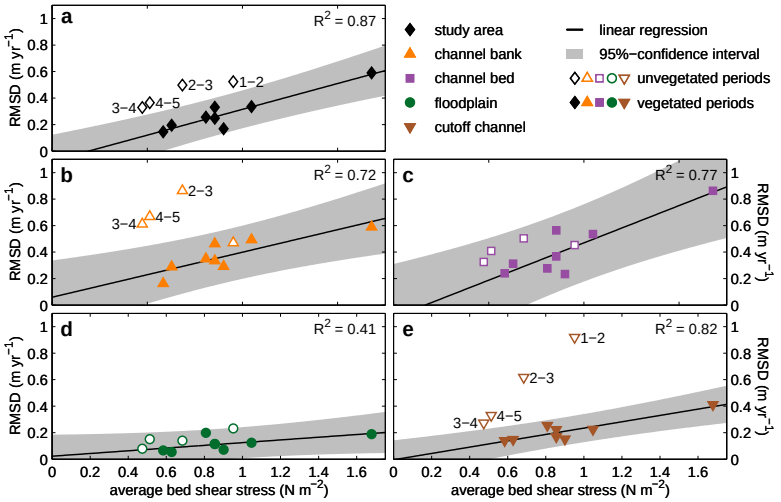

Fig. 11. Linear regression between time-averaged bed shear stress ($N\,m^{-2}$) and the root-mean-square elevation difference ($m\,yr^{-1}$), with **(a)** study area as a whole, **(b)** channel bank, **(c)** channel bed, **(d)** floodplain, and **(e)** cutoff channel. The delineated and coloured markers correspond to the unvegetated and vegetated period, respectively. The solid black lines denote the linear regression curves for the vegetated period (5–13). The grey-shaded areas indicate the extent of the 95 %-confidence interval of the regression model.